Atmos. Meas. Tech. Discuss., https://doi.org/10.5194/amt-2017-373
Manuscript under review for journal Atmos. Meas. Tech.
Discussion started: 17 October 2017

Atmospheric Measurement Techniques Discussions

Ice particle sampling from aircraft – influence of the probing position on the ice water content

Armin Afchine[1], Christian Rolf[1], Anja Costa[1], Nicole Spelten[1], Martin Riese[1], Bernhard Buchholz[2], Volker Ebert[2], Romy Heller[3], Stefan Kaufmann[3], Andreas Minikin[3], Christiane Voigt[3], Martin Zöger[3], Jessica Smith[4], Paul Lawson[5], Alexey Lykov[6], Sergey Khaykin[7], and Martina Krämer[1]

[1]Forschungszentrum Jülich, Institute for Energy and Climate Research (IEK-7), Jülich, Germany;
[2]PTB, Braunschweig, Germany;
[3]DLR, Wessling, Germany
[4]Harvard University, Cambridge, MA, USA
[5]SPEC Incorporated, Boulder, CO, USA
[6]Central Aerological Observatory (CAO), Department of Upper Atmospheric Layers Physics, Moscow, Russia
[7]LATMOS/IPSL, UVSQ Université Paris-Saclay, UPMC University Paris 06, CNRS, Guyancourt, France

Correspondence to: Martina Krämer (m.kraemer@fz-juelich.de)

Abstract. The ice water content (IWC) of cirrus clouds is an essential parameter determining their radiative properties and thus is important for climate simulations. Therefore, for a reliable measurement of IWC on board of research aircraft, it is important to carefully design the ice crystal sampling and measuring devices. During the HALO field campaign ML-CIRRUS in 2014, IWC was recorded by three closed path total water together with one gas phase water instrument. The hygrometers were supplied by inlets mounted on the roof of the aircraft fuselage. Simultaneously, the IWC is determined by a cloud particle spectrometer attached under an aircraft wing. Two more examples of simultaneous IWC measurements by hygrometers and cloud spectrometers are presented, but the inlets of the hygrometers were mounted at the fuselage side (Geophysica, StratoClim campaign 2017) and bottom (WB57, MacPex 2011). This combination of instruments and inlet positions provides the opportunity to experimentally study the influence of the ice particle sampling position on the IWC. As expected from theoretical considerations, we found that the IWCs provided by the roof inlets deviate from those measured under the aircraft wing. Caused by the inlet position in the shadow-zone behind the aircraft cockpit, ice particles populations with mean mass sizes larger than about 25 µm radius are subject to losses, which lead to strongly underestimated IWCs. On the other hand, cloud populations with mean mass sizes smaller than about 12 µm are dominated by particle enrichment and thus overestimated IWCs. In the range of mean mass sizes between 12 and 25µm, both enrichment and losses of ice crystal can occur, depending on whether the ice crystal mass peak of the - in these cases bimodal - size distribution is on the smaller or larger mass mode. The resulting deviations of the IWC reach factors of up to 10 or even more for losses as well as for enrichment. Since the mean mass size of ice crystals increases with temperature, losses are more pronounced at higher temperatures while at lower temperatures IWC is more affected by enrichment. In contrast, in the cases where the hygrometer inlets were mounted at the fuselage side or bottom, the agreement of IWCs is -due to undisturbed ice particle sampling, as expected from theory- most frequently within a factor of 2.5, independently of the mean ice crystal sizes. Summarizing, in case IWC needs to be detected

Atmos. Meas. Tech. Discuss., https://doi.org/10.5194/amt-2017-373
Manuscript under review for journal Atmos. Meas. Tech.
Discussion started: 17 October 2017

Atmospheric Measurement Techniques Discussions

solely by measurements from closed path hygrometers, it is crucial for a solid measurement to mount the respective inlets at the aircraft's side or bottom.

1 Introduction

Cirrus ice water content (IWC) is directly linked to the clouds extinction and thus relates bulk cloud properties to radiative properties (e.g. Gayet et al., 2004; Heymsfield et al., 2014; Thornberry et al., 2017). Since IWC is a parameter representing cirrus in global climate models, a solid knowledge of IWC is of importance. The most accurate measurements are achieved by in-situ aircraft observations where cirrus clouds are directly probed. However, the measurements must be carried out carefully to obtain the desired data quality. Beside the ability of the instruments that are used to detect the complete range of IWCs with sufficient accuracy, the probing position at the aircraft's fuselage is of importance (see Krämer et al., 2013, and references therein).

The IWC of a cirrus is a bulk quantity which is composed of the sum of all ice particles contained in an air volume. Depending on the position around the aircraft fuselage, there are shadow and enrichment zones for ice particles in dependence of the particles size. These zones are the most prominent particle measurement bias caused by an aircraft body. Thus, in case the position for particle sampling is placed in such a zone, it can be expected that an IWC measurement will be distorted. These effects are described already by airflow and trajectory calculations in King (1984). In particular, King (1984) shows that above the roof of an aircraft the sampling of particles is disturbed. However, to simulate and quantify losses or enrichment of ice particles and the effect on IWC at a specific position of an aircraft is hardly possible, since this depends on the prevailing particle size distribution and also the irregular shape of the ice crystals.

Here, we compare in-situ observations of IWC measured at the roof, side, bottom and under the wing of aircraft with different instruments to evaluate the influence of the particle probing position on cirrus IWC. Specifically, IWC is measured under the wing - which is the most favorable position for particle sampling - during three field campaigns with differing aircraft. One aircraft is in addition equipped with three other IWC instruments placed at the aircraft roof, at the second the IWC measurements are placed at the aircraft side and at the third at the aircraft bottom. From comparison of the correlation of the roof, side and bottom to the wing IWCs conclusions are drawn about the representativeness of the measurement at the specific position.

2 IWC measurements - a brief excursion into theory

The IWC of cirrus can be recorded from aircraft either by bulk cloud measurements using airborne closed path hygrometers mounted behind an inlet tube or via integration of the ice particle number size distributions (PSD_{ice}) measured by cloud spectrometers. In both cases, the ice particles must be properly sampled before the measurement. The bulk IWC is less error-prone in comparison to the IWC from PSD_{ice} in case of an undisturbed measurement. The reason is that before the bulk measurements the ice crystals are evaporated while the size resolved IWC detection must account for the ice crystal shapes.

Atmos. Meas. Tech. Discuss., https://doi.org/10.5194/amt-2017-373
Manuscript under review for journal Atmos. Meas. Tech.
Discussion started: 17 October 2017

Atmospheric Measurement Techniques Discussions

In the following, a brief summary on sampling and measuring IWC on fast flying aircraft is given. Fore more detail, we refer to e.g. Krämer and Afchine (2004), Schiller et al. (2008), Wendisch and Brenguier (2013), Krämer et al. (2013), Luebke et al. (2013).

2.1 IWC from hygrometers

The bulk IWC is derived from the difference between H_2O_{tot}, which is the amount of total water (H_2O_{gas} + evaporated ice crystals) contained in a cirrus, and H_2O_{gas}, the gas phase water amount. The IWC is calculated by using the following Equation:

$$IWC = H_2O_{tot} - H_2O_{gas} = \frac{H_2O_{enh} - H_2O_{gas}}{E_{max}} \quad (1)$$

where H_2O_{enh} (H_2O_{tot} enhanced by an oversampling of ice crystals) and E_{max} (enhancement factor) are parameters related to the sampling of the ice crystals by an inlet tube which is described in Section 2.1.2.

For the measurement of H_2O_{gas}, the air loaden with water vapor is passed into the aircraft by an inlet tube which faces against the direction of flight. Therefore, a pump is used to suck the air through the inlet-hygrometer-exhaust line. No cloud particles enter backward facing inlets, since their inertia is too high for a complete U-turn. The hygrometer is mounted behind the inlet in the aircraft cabin.

To measure H_2O_{tot}(or H_2O_{enh}, respectively) is more difficult, since also ice particles of a wide range of sizes ($\approx$ 3 – 1000 µm or more in cirrus clouds) has to be passed into the aircraft. To this end, inlet tubes facing into the direction of flight are deployed. To precisely detect H_2O_{tot}, the ice crystals have to be completely evaporated before they enter the hygrometer, which is placed subsequently in the sampling line. To this end, the inlet should be heated to up to 90°. In addition, a strong bend should follow directly behind the inlet to shatter ice crystals to small fragments that evaporate in a short time. Behind the water measurement the air leaves the aircraft at the outlet point. Most systems are so-called 'free stream' sampling lines, i.e. the flow is generated by the pressure difference between the inlet tip and the outlet. Prerequisite for a reliable H_2O_{tot} measurement is a suitable, well-characterized inlet so that the true concentration of water plus evaporated ice crystals can be determined. To accomplish this requirements, two points are important: (i) First, the inlet needs to be placed at the aircraft fuselage in a way to enable sampling in undisturbed flow. (ii) Further, the inlet itself should not influence the gas phase water and ice particle concentration. These two points are briefly described in the following, mainly based on Krämer et al. (2013) and references therein.

2.1.1 IWC enrichment or loss due to inlet position

The principle behavior of gas streamlines and cloud particle trajectories around an aircraft fuselage can be seen in Figure 1 (adapted from King, 1984). In the upper panel of these early, but still meaningful potential flow simulations, the predicted gas flow streamlines at 90 m/s are displayed. Far in front of the aircraft's nose they are equally spaced, indicating the same flow velocity. However, due to the aircraft body the streamlines are compressed over the cockpit, indicating regions of higher

Atmos. Meas. Tech. Discuss., https://doi.org/10.5194/amt-2017-373
Manuscript under review for journal Atmos. Meas. Tech.
Discussion started: 17 October 2017

Atmospheric Measurement Techniques Discussions

airspeed -and also enriched concentrations of smaller cloud particles that follow the streamlines- (right side) compared to the free stream.

In the bottom panel, trajectories for larger (exemplarily 100 µm) cloud particles are displayed for the same flight conditions. As these particles have high inertia, most of the trajectories end at the aircraft fuselage, i.e., the particles impact on the aircraft. However, some of the trajectories were deviated, leading to regions devoid of particles (shadow zone) or with increased particle concentration (enrichment zone).

To specify the size ranges of the 'smaller' and 'larger' cloud particles, CFD calculations for the specific conditions of fuselage shape, aircraft speed and inlet distance from the nose of the aircraft need to be performed. Very roughly, cloud particles with radii $<$30 µm can be assumed to belong to the smaller, while those $>$30 µm are associated to the larger part of the cloud particle size spectrum at jet aircraft with high air speeds. Altogether, when measuring cloud particles it is important to know where shadow and enrichment zones on the aircraft platform are located, since at the same fuselage station it is possible to sample in the shadow/enrichment zone for larger/smaller particles if a probe is positioned close to the aircraft fuselage or in the enrichment zone for larger particles in case the probe is farther away from the fuselage.

2.1.2 IWC enhancement due to inlet design

The first requirements to an inlet for a proper sampling are that it protrudes beyond the aircraft boundary layer and that the wall of the inlet tip is thin enough to avoid strong shattering of ice crystals or deviation of streamlines from the free flow. However, isokinetic sampling (= the flow inside the inlet is the same as in the free flow), which in principle enables the undisturbed measurement of H_2O_{tot}, is not possible for fast flying aircraft, since the air flow speed is always much higher than the velocity inside of the inlet. Such inlet types are called 'nearly virtual impactors', since the velocity inside of the inlet tube is so small that the inlet cross section appears like an impaction plate. Such inlets sample strongly 'subisokinetic', i.e. the part of the cross section where gas streamlines enter the inlet is much smaller than the part of the cross section that samples ice particles. The particle sampling cross sections increases with increasing particle size up to the total inlet cross section for the largest particles. As a consequence, ice crystals are sampled from a much larger (enhanced) air volume than H_2O_{gas} and thus the combined sampling of H_2O_{gas} and evaporated ice crystals is also enhanced (H_2O_{enh} instead of H_2O_{tot}). To adjust the two volumes to each other, the ice crystal air volume (and thus the IWC, see Eq. 1) needs to be corrected for this enhancement.

As mentioned, the enhancement (which can also be called 'aspiration efficiency') is dependent on particle size and increases for larger particles, up to a maximum value E_{max}. This maximum value is used for the calculation of the IWC (see Eq. 1). E_{max} can be calculated from the velocity of the free stream (i.e. the aircraft speed U_0) and the velocity U inside of the inlet:

$$E_{max} = \frac{U_0}{U} \tag{2}$$

The point where the enhancement is 50% of E_{max} (E_{50}) is called the 'cut-off' size of the inlet which defines the particle size range sampled by the inlet. E_{max} is dependent on U, which in turn depends, among other parameters like pressure, temperature and aircraft speed U_0, strongly on the pressure difference between inlet and outlet, the driving force of the flow. Thus, U decreases with increasing altitude.

Atmos. Meas. Tech. Discuss., https://doi.org/10.5194/amt-2017-373
Manuscript under review for journal Atmos. Meas. Tech.
Discussion started: 17 October 2017

Atmospheric Measurement Techniques Discussions

With the knowledge of E_{max}, the IWC can now be calculated following Eq. 1 and H_2O_{tot} consequently is H_2O_{gas}+IWC. In Figure 2, we visualize the complex relation between the measuring parameter H_2O_{enh}, IWC and E_{max} in dependence of temperature for given H_2O_{gas} (assumed as the saturation value for the calculations), calculated from Eq. 1 (left column: E_{max} = 10, right column: E_{max} = 50; top row: volume mixing ratio, bottom row: concentration). To avoid very small artificial IWCs caused by the uncertainties of measurements and not by ice particles, the minimum difference between H_2O_{enh} and H_2O_{gas} needs to be to 5% to encounter an IWC. The differently colored regions show the ranges of H_2O_{enh} and IWC belonging to each another. It can be seen from Figure 2, that the IWCs covered by H_2O_{enh} of the same color are broader and show lower IWCs at higher temperatures and narrower with higher IWCs at lower temperatures. This reflects the fact that H_2O_{gas} decreases with temperature and is thus stronger enhanced due to the addition of ice crystals. Consequently, H_2O_{enh} 'jumps' to a higher value with another color. Regarding the difference between E_{max} = 10 and 50 (left and rights panels of Figure 2) it becomes visible that the higher E_{max}, the smaller the IWCs that can be detected.

The range of IWCs that can be detected with a H_2O_{tot} instrument can be seen from Figure 2. The blue H_2O_{enh} isolines through the IWC-T parameter space correspond to the detection limit of an instrument, e.g. the '1ppmv' and '3ppmv' H_2O_{enh} isolines represent the IWC detection limit of the FISH and HAI instruments that will be described in Section 3.1.2. Further, the IWC detection range is limited at the lower end of IWC in dependence of temperature by the requirement that $H_2O_{enh}/H_2O_{gas} > 1.05$. A difference of 5% between the two measurements is necessary to avoid that artificial clouds emerge caused by the scatter of the instruments (see also Schiller et al., 2008).

2.2 IWC from cloud spectrometers

Cloud spectrometers measure the cloud particle number size distribution PSD_{ice}. They are in most cases mounted below the the aircraft wings with sufficient distance to the wing and the aircraft body to minimize particle losses or enrichment due to distorted cloud particle trajectories or contamination by cloud particles bounced from the air frame (Krämer et al., 2013). In any case, deviations of streamlines does not play a great role in the flow around wings. To avoid uncertainties in the measurements caused by the aircraft's angle of attack, the cloud probes should be mounted under this angle to compensate this effect. Ice crystal shattering into small artifacts at the cloud probes head is a source of error in PSD_{ice}. However, for the calculation of the IWC, the uncertainty from shattering does not play a significant role since the shattered crystals still contribute to the integrated mass of PSD_{ice}. In addition, newer cloud spectrometers are designed in order to minimize shattering, and anti-shatter algorithms can account ice fragments stemming from large shattered ice crystals (Korolev et al., 2011). Other measurement issues of PSD_{ice} are discussed in detail in (Krämer et al., 2013) and Baumgardner et al. (2017).

The IWC is derived from PSD_{ice} by summing up the ice crystal concentrations measured in each size bin of the number size distribution. The largest source of error in this method is the irregularity of the ice crystal shapes. Especially large ice crystals cannot be assumed as spheres and their shapes strongly vary. Numerous so-called mass-dimension (m–D) or mass-area (m-A) relations are derived to account for this effect. A summary of m-D relations is given e.g. in Abel et al. (2014) and a new,

Atmos. Meas. Tech. Discuss., https://doi.org/10.5194/amt-2017-373
Manuscript under review for journal Atmos. Meas. Tech.
Discussion started: 17 October 2017

Atmospheric Measurement Techniques Discussions

advanced relation is developed by Erfani and Mitchell (2016). The m–D relations are of the form:

$$m_i = a \cdot D_i^b \tag{3}$$

with m_i,D_i mass and diameter of the ice crystals of the i-th size bin and a, b constants of respective relations. The IWC is then:

$$IWC = \sum_{i=1}^{n} m_i \cdot dN_i \tag{4}$$

3 IWC instrumentation

3.1 Bulk IWC inlet and hygrometers

3.1.1 H_2O_{tot} inlets

For the HALO aircraft, Trace Gas Inlets (TGI) are designed[1], mainly to probe atmospheric gas components, but also to sample ice cloud particles. The design can be seen in the bottom panel of Figure 3, where a TGI is mounted with three inlets facing in forward direction for cloud sampling and one inlet in backward direction for gas constituents. The TGI inlet is heated, and the sampling tubes have a 90° bend as required to evaporate ice crystals entering the forward facing ducts (see Section 2.1.) During ML-CIRRUS in 2014, two TGIs were mounted on the frontmost apertures of HALO's roof. The roof position was chosen for the various apertures due to technical restrictions. Two H_2O_{tot} hygrometers (FISH and Waran, for description of the H_2O instruments see next section) are positioned at the upper forward inlet tips of TGI 1 and 2, a third hygrometer (HAI) is connected to the middle forward duct of the TGI 1. The TGI position at the aircraft fuselage is shown in the top panel of Figure 3. The hygrometer used for H_2O_{gas} sampling (SHARC) is connected to a backward inlet tip of a TGI mounted above the wings.

On board of Geophysica, the inlet for the H_2O_{tot} hygrometer FISH is mounted at the side of the aircraft, as can be seen in Figure 4. It is also heated and has a 90° bend. The H_2O_{gas} hygrometer FLASH is mounted below a wing and equipped with it's own inlet. The WB-57 H_2O_{tot} inlet for the FISH hygrometer is mounted at the aircraft's bottom (see Figure 5) and is as well heated and has a 90° bend. The H_2O_{gas} hygrometer HWV is mounted below a wing and equipped with it's own inlet. The IWCs derived from the H_2O_{tot} measurements behind the respective inlets are here referred to as roof, side and bottom IWCs.

3.1.2 H_2O instruments

The essentials of the hygrometers used to measure H_2O_{tot} and H_2O_{gas} on board of HALO during ML-CIRRUS 2014 (FISH, HAI, Waran and SHARC) are summarized in the following. For more detail we refer to the respective cited publications of the instruments.

[1] *enviscope* GmbH.

Atmos. Meas. Tech. Discuss., https://doi.org/10.5194/amt-2017-373
Manuscript under review for journal Atmos. Meas. Tech.
Discussion started: 17 October 2017

Atmospheric Measurement Techniques Discussions

FISH (Fast In situ Stratospheric Hygrometer) is a closed path Lyman-α photofragment fluorescence (Zöger et al., 1999; Meyer et al., 2015) to measure H_2O_{tot} in the range of 1- 1000 ppmv between 50-500 hPa with an accuracy/precision of 6–8%/0.3 ppmv. Connected to the HALO-TGI forward facing duct, the enhancement factor range is 12-20. In accordance to Figure 2, the resulting minimum detectable IWC is between about 1-20·10^{-3} ppmv ($\sim$ 1-20·10^{-4} mg/m^3).

HAI (Hygrometer for Atmospheric Investigation) is a four channel Tunable Diode Laser hygrometer (Buchholz et al., 2017). Here, we use its closed path 1.4 µm H_2O_{tot} channel, for brevity called HAI in the following. The measurement range is 3 - 40000 ppmv with an accuracy/precision of 4.3%$\pm$3 ppmv/0.24 ppmv. Its enhancement factor at the HALO-TGI is 17-50, the resulting minimum IWC following Figure 2 is between about 0.5-20·10^{-2} ppmv ($\sim$ 0.5-20·10^{-3} mg/m^3).

Waran (Water Vapor Analyzer) is a tunable diode laser hygrometer (1.4 µm) WVSS (Vance et al., 2015), attached to the forward facing TGI (Voigt et al., 2017) instead of the originally associated inlet. The detection range is $\gtrsim$50–40000 ppmv, the accuracy according to the manufacturer is $\pm$50 ppmv or 5% of reading, whatever is larger. However, good performance of WVSS down to about 20 ppmv is reported in Smit et al. (2013) in a comparison of airborne hygrometers. The enhancement factor at the HALO-TGI is in the range of 20-35 and the resulting minimum detectable IWC is (see Figure 2) between about 0.5-50·10^{-1} ppmv (0.5-50·10^{-2} mg/m^3).

SHARC (Sophisticated Hygrometer for Atmospheric Research) is also a closed path Tunable Diode Laser hygrometer (1.4 µm), but at HALO used for H_2O_{gas} measurements (Meyer et al., 2015). Its range of detection is 20-40000 ppmv with an accuracy/precision of 2-4%/0.2 ppmv.

On board of Geophysica during StratoClim 2017, H_2O_{tot} was measured by FISH, while for H_2O_{gas} FLASH (FLuorescent Airborne Stratospheric Hygrometer, for details see Khaykin et al., 2013) was used. FLASH uses also the Lyman-α photofragment fluorescence technique for the detection of water vapor, but its inlet is designed to sample only the gas phase.

FISH was also used for H_2O_{tot} measurements on board of the WB-57 during MacPex 2011. In this case, H_2O_{gas} is detected by the Lyman-α fluorescence hygrometer HWV (Harvard Water Vapor). Details of the water measurements during MacPex are described in Rollins et al. (2014).

3.2 Cloud spectrometers for IWC

During ML-CIRRUS 2014 and also StratoClim 2017, the NIXE-CAPS (New Ice eXpEriment: Cloud and Aerosol Particle Spectrometer, NIXE hereafter) instrument, mounted under the wing of HALO (see Figure 6) and Geophysica, respectively, was used to measure the cloud particle number size distribution in the size range of 3-930 µm diameter (Meyer, 2012). Two instruments are incorporated in NIXE: the NIXE-CAS-DPOL (Cloud and Aerosol Spectrometer with Detection of POLarization) and the NIXE-CIPg (Cloud Imaging Probe - Greyscale). In combination, particles with diameters between 0.61 µm and 937 µm can be sized and counted. For cloud measurements, particle diameters $>$ 3 µm are considered. The IWC was derived using the m-D relation described by Krämer et al. (2016) and Luebke et al. (2016). This relation, originally derived from observations by Mitchell et al. (2010) and confirmed in the study of Erfani and Mitchell (2016), has nearly no dependency on temperature

or cirrus type, thus demonstrating the robustness of the connection between cirrus ice crystal size and mass. In Section 4.1.3, the m-D relation is again confirmed by measurements (see also Figure 9, left panel).

During MacPex 2011, the cloud spectrometer 2D-S (Lawson et al., 2006) was mounted under the wing of the WB-57 to measure cloud particles. 2D-S is an optical imaging cloud probe comparable to the CIPg, covering the particle size range of 15-1280 µm diameter. The IWC is derived from an a-D (area-dimension) relation described by Baker and Lawson (2006) which is again confirmed here (see Section 4.1.3 and Figure 9, right panel).

The IWCs derived from the wing mounted NIXE or 2D-S ice particle measurements are here referred to as 'Wing IWCs'.

4 Ice particle probing position and IWC

4.1 IWCs from roof/side/bottom and wing sampling

4.1.1 Roof H_2O measurements

First, the measurements of the hygrometers mounted at roof of the HALO aircraft (FISH, HAI, Waran and SHARC) are compared to each other to ensure that possible instrument differences are not attributed to the probing position in the further discussion. To this end, scatter plots of H_2O in clear air as well as IWCs in cirrus are shown in Figure 7. Good agreement of the clear air H_2O measurements (at $RH_{ice} < 60\%$ to strictly exclude clouds) from FISH, HAI and SHARC is demonstrated in the left panel of the figure. The middle panel show the IWC scatter plot of FISH and HAI. Most of the measurements symmetrically spread around the 1:1 line by a factor of 2.5, which can be considered as a good agreement. In the right panel, the measurements of FISH and Waran are displayed. The data are mostly placed above the 1:1 line, most frequently around a factor of 2. This means that the IWC of Waran is shifted to higher values in comparison to FISH. An explanation for this behavior is still missing. IWCs below about 0.5 ppmv are not detected by Waran, showing the smaller IWC range of Waran (see Section 3.1.2).

4.1.2 Roof and wing IWCs

IWCs from measurements at the aircraft roof in comparison to the IWC measured under the wing are shown in Figure 8. The left/middle/right panels of the figure depict roof-mounted FISH/HAI/WARAN versus wing-mounted NIXE observations.

The first to note is the relatively broad scatter of all IWC measurements. This can be seen from the broad distribution of the data points between the black dashed lines in the panels, which represent a factor of ± 10 to the black solid 1:1 line. A closer look to the panels by taking notice of the frequencies of occurrence (see color code in the figure), however, shows narrower structures parallel to the 1:1 lines. For the FISH instrument, at medium IWCs most data pairs are placed above the 1:1 line (IWC enrichment), while at higher IWCs the highest frequencies are found below the line (IWC losses). The same is found for HAI, but at medium IWC losses are seen more often than for FISH. Vice versa, for Waran an IWC enrichment is more abundant in the medium IWC range.

Atmos. Meas. Tech. Discuss., https://doi.org/10.5194/amt-2017-373
Manuscript under review for journal Atmos. Meas. Tech.
Discussion started: 17 October 2017

Atmospheric Measurement Techniques Discussions

4.1.3 Side/bottom and wing IWCs

To investigate if the differences of the IWCs from roof and wing measurements found in the last section might be indeed related to the H_2O_{tot} inlet position at the aircraft's roof, we analyze IWCs correlations of side/wing and bottom/wing measurements in the following.

Side IWCs were measured by FISH (H_2O_{tot}, see inlet position in Figure 4) together with the hygrometer FLASH for H_2O_{gas}, while wing IWCs are recorded by the cloud spectrometer NIXE during the recent field campaign StratoClim 2017 (http://www.stratoclim.org/) with the Russian aircraft Geophysica. Under clear sky conditions the hygrometers agree as well as those shown in Figure 7, left panel (not shown here).

A good agreement of side/wing IWCs can be seen from the left panel of Figure 9. The majority of data pairs distribute here between the thin lines, representing a factor of ± 2.5. Since for these measurements the same instruments as for the roof/wing measurements were used for ice particle sampling, the position of the H_2O_{tot} inlet at the side of the aircraft is most probably the cause for the better agreement of the IWCs in comparison to the roof/wing IWCs discussed in the previous section. The reason is that here the airflow clings along the aircraft fuselage because the cockpit does not disturb it. Consequently, the trajectories of the ice crystals are not deflected, as it occurs at the roof of the aircraft (see Section 2). Another aspect of the good agreement between the two measurements is that it shows the validity of the m-D relation used to calculate the IWC from the PSD_{ice} measured by NIXE.

Bottom and wing IWCs were measured by FISH for H_2O_{tot} (see see inlet position in Figure 5) and the hygrometer HWV for H_2O_{gas}, together with the cloud spectrometer 2D-S, mounted at the US aircraft WB-57 during the field campaign MacPex 2011 (see Krämer et al., 2016). FISH and HWV agreed also well under clear sky conditions, as demonstrated in Figure 7, left panel (not shown here).

It can be seen from Figure 9, right panel, that - beside that mostly high IWCs are found in the probed mesoscale convective cloud systems - the bottom/wing data pairs are also evenly distributed around the 1:1 line as for the side/wing observations. This is again attributed to the position of the H_2O_{tot} inlet at the bottom of the aircraft where the ice crystals are not deflected.

In both cases, side and bottom ice particle sampling position, the data distributes around the 1:1 line mostly in between a factor of ± 2.5, represented by the thin lines. This is in good agreement with a study of de Reus et al. (2009), where IWCs from H_2O_{tot} (FISH and FLASH) and cloud spectrometers (FSSP and CIP) measurements at the Russian aircraft Geophysica are compared during the field campaign SCOUT-O_3. de Reus et al. (2009) reported an IWC scatter of ± 2.2 around the 1:1 line. A scatter of IWC data in this order of magnitude is also reported by Thornberry et al. (2017), who measured IWCs by means of the side mounted NOAA-TDL hygrometer and the wing mounted cloud spectrometers FCDP and 2D-S on board of the Global Hawk during the ATTREX 2014 campaign.

Atmos. Meas. Tech. Discuss., https://doi.org/10.5194/amt-2017-373
Manuscript under review for journal Atmos. Meas. Tech.
Discussion started: 17 October 2017

4.2 Impact of ice crystal size on roof IWC

To further investigate the structures seen in the roof/wing IWC scatter plots discussed in Section 4.1.2 (see Figure 8), we analyze the influence of the ice particle size distribution (PSD_{ice}) on the IWCs. To this end, we look at the ratio of the roof to the wing IWCs in dependence of the mean mass radius R_{ice} of the PSD_{ice} (R_{ice} = IWC/N_{ice} from NIXE, N_{ice} = total number of ice crystals > 3 µm). The results are shown in Figure 10. In case of undisturbed sampling at both positions at the aircraft, the distribution of the data points should be homogeneous around the 1-line of the IWC-ratio, with the highest frequencies closest to this line. However, the data distribution are more 'duck' shaped for all three roof-mounted H_2O_{tot} instruments. The appearance of the IWC ratios can be divided in three regimes, marked by the thin vertical red lines in Figure 10.

(1) An 'enrichment regime' is observed for small R_{ice} (about < 12 µm). A mass size distribution typical for this regime is displayed in Figure 11 (PSD_{ice} 1, top panel; note that for the portrayal of the PSD we use the ice particle diameter and not radius to clearly distinguish from the mean mass radius R_{ice} of the ice particle population used in Figures 10). The ice mass accumulates at smaller sizes, larger ice particles does not contribute to the IWC. Following Section 2 (Figure 1), smaller ice crystals at the aircraft roof are enriched close to the fuselage and this is what Figure 10 demonstrates. Further, this is consistent with the enrichment at lower IWC seen in Figure 8.

(2) An 'even-handed regime' is found for intermediate R_{ice} (about 12-25 µm). The corresponding typical PSD_{ice} 2 can be seen in the middle panel of Figure 11. This type of PSD_{ice} is bimodal with one ice mass peak at smaller and another at larger sizes. Depending on which of the peaks is dominating, the accumulation of smaller ice crystals in the aircraft's enrichment zone or the losses of larger ice crystals in the shadow zone overbalance.

(3) A 'loss regime' is detected for large R_{ice} (about $\gtrsim 25$ µm). Here, the large ice crystals connected to PSD_{ice} 3 shown in Figure 11 are not sampled in the shadow zone at the aircraft roof. The losses of roof IWC at higher IWCs shown in Figure 8 correspond to this regime.

The 'duck' shape of the IWC ratios of the three instruments slightly differ from each other. Most equally distributed around the ratio 1 are the FISH/NIXE IWCs (top panel of Figure 10), with the highest frequencies in the enrichment part of the 'even-handed regime' at IWC ratios slightly above 1. HAI/NIXE IWC ratios (middle panel of Figure 10) on the other hand have the highest frequencies in the loss part of the 'even-handed regime' reaching IWC ratios significantly below 1. This is consistent with the fact that the HAI instrument is connected to the middle forward inlet (see Figure 3) and is thus -in comparison to the FISH inlet- closer to the fuselage. Here, the losses of large particles are more pronounced. Notable is that already a few centimeter have such a large effect on the particle sampling efficiency. The bottom panel of Figure 10 shows the Waran/NIXE IWC ratios. Waran is connected -as FISH- to the roof inlet of a TGI right next to that of FISH and thus shows a comparable distribution of frequencies, but shifted to higher values. This reflects that the Waran IWCs are in general somewhat higher than those of the other instruments (see Figures 7 and 8).

Atmos. Meas. Tech. Discuss., https://doi.org/10.5194/amt-2017-373
Manuscript under review for journal Atmos. Meas. Tech.
Discussion started: 17 October 2017

Atmospheric Measurement Techniques Discussions

4.3 Roof and wing IWC climatologies

An overview of the impact of the sampling position on the IWC is given in Figures 12, where IWC frequencies of occurrence are shown in dependence of temperature for the roof-mounted FISH instrument (top panel) and the wing-mounted NIXE (bottom panel).

Comparing the roof and wing IWCs at warmer temperatures, it can be clearly seen that high IWCs are not measured at the roof position and thus the higher frequencies are shifted to lower IWCs. The reason is that high IWCs at temperatures $\gtrsim$ 220 K are related to large ice crystal sizes belonging to the 'loss regime' discussed in the previous section, which can be seen in Figures 12 (bottom panel), where frequencies of occurrence of R_{ice} in dependence of temperature are plotted. At lower temperatures, the mean mass ice crystal sizes R_{ice} shrinks into the 'even-handed' and 'enrichment regime' that means they are often enriched, resulting in an overestimation of the roof IWCs. This can be seen in the higher frequencies of larger roof IWCS in comparison to the wing IWCs.

Altogether, the IWC climatology of the roof IWCs covers roughly the same range as that of the wing IWCs, with the exception that large IWCs at high temperatures are missed. However, the distribution of the frequencies of occurrence of the IWCs is, caused by the position of the H_2O_{tot} inlet, heavily skewed for the roof IWCs.

5 Summary and conclusions

IWC is measured at three positions of aircraft fuselages, roof, side and bottom, as well as under the wing. The measurements show a satisfactory good agreement between side/bottom and wing IWCs, most frequently they correspond to each other within a factor of 2.5, independently of the mean ice crystal sizes. This is because under the aircraft wing and at the side and bottom of the fuselage, the cirrus cloud particle trajectories are not greatly diverted caused by the aircraft body or the wing itself, so that the sampling of ice crystals represent nearly ambient conditions.

In addition, the agreement of the IWCs does not only show the performance of the side, bottom and wing sampling position, but also the agreement of the IWC instrumentation. This is notable since the measurement techniques greatly differ, the side/bottom IWC is measured by the Lyman–α fluorescence hygrometer FISH and the wing IWC is obtained from the ice particle mass size distribution measured by optical methods with NIXE-CAPS and 2D-S. A further conclusion from the agreement of the IWCs is that it demonstrates the validity of the m-D relation of Erfani and Mitchell (2016), slightly modified by Krämer et al. (2016) and Luebke et al. (2016), which is applied to convert the NIXE-CAPS size of the ice crystals into mass.

However, roof and wing IWCs differ from each other. The reason is that the cockpit causes deviations of the streamlines and particle trjectories above the roof, leading to both, enrichment and losses of particles depending on the size of the ice particles. Large ice particles are lost in the shadow-zone behind the aircraft's cockpit, while at the same time smaller ice crystals are enriched. For mean mass radii of the ice particle population smaller than about 12 µm (range 2 - 100 µm), enrichment of the ice crystals and thus an overestimation of the IWC dominates. In the size range 12 to about 25 µm both enrichment and losses of ice crystal occurs, while loss of large crystals leading to strongly underestimated IWCs prevails for larger sizes. Enrichment and losses are in the order of a factor of 10 or more.

A correction of the IWCs measured at aircraft roofs might only be possible when ice particle PSDs are measured simultaneously. However, in that case the IWCs calculated from the PSDs would still be more accurate. Because of the high variability of the ice particle size distributions, it is also not an option to assume PSDs, e.g. in dependence of temperature, for a correction of the roof IWCs.

The influence of the size dependent enrichment or losses of ice crystals from roof sampling propagates to IWC climatologies with respect to temperatures. At higher temperatures, where the ice crystals are larger, IWCs are underestimated due to the ice particle losses, while at lower temperatures overestimation of IWC caused by particle enrichment dominates.

The recommendations resulting from this comparison of in-situ measurements of IWC are that (i) reliable measurements of IWC are possible from sampling positions at the side, bottom and under the wing when using (ii) instruments with a detection range that cover the complete wide IWC range from about 0.001 to 3000 ppmv. The best approach to measure IWC is to deploy a combination of two instruments at different sampling positions. As last remark we like to note that this recommendations also applies to other ice particle measurements, such as ice crystal numbers sampled by counterflow virtual impactors (Mertes et al., 2007).

Author contributions.

A. Afchine: NIXE-CAPS measurements and IWC analysis; M. Krämer: FISH and NIXE-CAPS measurements, IWC analysis; C. Rolf: FISH measurements and IWC analysis; A. Costa: NIXE-CAPS measurements; N. Spelten: FISH measurements; M. Riese: FISH and NIXE deployment; B. Buchholz: HAI measurements; V. Ebert: HAI measurements; R. Heller: Waran measurements; S. Kaufmann: Waran measurements; C. Voigt: Waran measurements; M. Zöger: SHARC measurements; P. Lawson: 2D-S measurements; J. Smith: HWV measurements; A. Lykov: FLASH measurements; S. Khaykin: FLASH measurements ; A. Minikin: under wing cloud spectrometer configuration.

Acknowledgements. The authors would like to thank the DFG (Deutsche Forschungsgemeinschaft, German Research Foundation) Priority Program SPP 1294 for funding of the FZJ project 'ACIS' (KR 2957/1-1) and the PTB HAI project (EB 235/3-1 and EB 235/3-2). C. Voigt thanks for finding by HGF contract No. W2/W3-60 and by DFG SPP HALO 1294 contract No. V01504/4-1. Special thanks to our colleagues S. Mertes (TROPOS, Leipzig) and H. Ziereis (DLR, Wessling) for stimulating and important discussions on the topic of ice crystal sampling from aircraft roof.

References

Abel, S. J., Cotton, R. J., Barrett, P. A., and Vance, A. K.: A comparison of ice water content measurement techniques on the FAAM BAe-146 aircraft, Atmospheric Measurement Techniques, 7, 3007–3022, https://doi.org/10.5194/amt-7-3007-2014, https://www.atmos-meas-tech.net/7/3007/2014/, 2014.

Baker, B. and Lawson, R. P.: Improvement in determination of ice water content from two-dimensional particle imagery. Part I: Image-to-mass relationships, JOURNAL OF APPLIED METEOROLOGY AND CLIMATOLOGY, 45, 1282–1290, https://doi.org/10.1175/JAM2398.1, 2006.

Baumgardner, D., Abel, S. J., Axisa, D., Cotton, R., Crosier, J., Field, P., Gurganus, C., Heymsfield, A., Korolev, A., Krämer, M., Lawson, P., McFarquhar, G., Ulanowski, Z., and Um, J.: Cloud Ice Properties: In Situ Measurement Challenges; Chapter 9 of 'Ice Formation and Evolution in Clouds and Precipitation: Measurement and Modeling Challenges', Meteorol. Monographs, https://doi.org/10.1175/AMSMONOGRAPHS-D-16-0011.1, 2017.

Buchholz, B., Afchine, A., Klein, A., Schiller, C., Krämer, M., and Ebert, V.: HAI, a new airborne, absolute, twin dual-channel, multi-phase TDLAS-hygrometer: background, design, setup, and first flight data, ATMOSPHERIC MEASUREMENT TECHNIQUES, 10, 35–57, https://doi.org/10.5194/amt-10-35-2017, 2017.

de Reus, M., Borrmann, S., Bansemer, A., Heymsfield, A., Weigel, R., Schiller, C., Mitev, V., Frey, W., Kunkel, D., Kürten, A., Curtius, J., Sitnikov, N., Ulanovsky, A., and Ravegnani, F.: Evidence for ice particles in the tropical stratosphere from in-situ measurements, Atmos. Chem. Phys., 9, 67756792, 2009.

Erfani, E. and Mitchell, D. L.: Developing and bounding ice particle mass- and area-dimension expressions for use in atmospheric models and remote sensing, Atmospheric Chemistry and Physics, 16, 4379–4400, https://doi.org/10.5194/acp-16-4379-2016, https://www.atmos-chem-phys.net/16/4379/2016/, 2016.

Gayet, J.-F., Ovarlez, J., Shcherbakov, V., Ström, M., Schumann, U., Minikin, A., Auriol, F., Petzold, A., and Monier, M.: Cirrus cloud microphysical and optical properties at southern and northern midlatitudes during the INCA experiment, J. Geophys. Res., 109, D20206, https://doi.org/10.1029/2004JD004803, 2004.

Heymsfield, A. J., Winker, D., Avery, M., Vaughan, M., Diskin, D., Deng, M., Mitev, V., and Matthey, R.: Relationships between ice water content and volume extinction coefficient from in situ observations for temperatures from 0° to 86°C: Implications for spaceborne lidar, J. Appl. Meteorol. Climatol., 53, 479–505, https://doi.org/10.1175/JAMC-D-13-087.1, 2014.

Khaykin, S. M., Engel, I., Vömel, H., Formanyuk, I. M., Kivi, R., Korshunov, L. I., Krämer, M., Lykov, A. D., Meier, S., Naebert, T., Pitts, M. C., Santee, M. L., Spelten, N., Wienhold, F. G., Yushkov, V. A., , and Peter, T.: Arctic stratospheric dehydration – Part 1: Unprecedented observation of vertical redistribution of water, Atmos. Chem. Phys., 13, 11 503 – 11 517, https://doi.org/10.5194/acp-13-11503-2013, 2013.

King, W. D.: Air flow and particle trajectories around aircraft fuselages I: Theory, J. Atmos. Ocean. Techn., 1, 5–13, 1984.

Korolev, A., Emery, E., Strapp, J., Cober, S., Isaac, G., Wasey, M., and Marcotte, D.: Small ice particles in tropospheric clouds: fact or artifact? Airborne Icing Instrumentation Evaluation Experiment, Bull. Am. Meteorol. Soc., 92, 967–973, https://doi.org/10.1175/2010BAMS3141.1, 2011.

Krämer, M. and Afchine, A.: Sampling characteristics of inlets operated at low U/U0 ratios: new insights from computational fluid dynamics (CFX) modeling, J. Aerosol Sci., 35, 683 – 694, 2004.

Krämer, M., Rolf, C., Luebke, A., Afchine, A., Spelten, N., Costa, A., Meyer, J., Zoeger, M., Smith, J., Herman, R. L., Buchholz, B., Ebert, V., Baumgardner, D., Borrmann, S., Klingebiel, M., and Avallone, L.: A microphysics guide to cirrus clouds - Part 1: Cirrus types, Atmospheric Chemistry and Physics, 16, 3463–3483, https://doi.org/10.5194/acp-16-3463-2016, 2016.

Krämer, M., Twohy, C., Hermann, M., Afchine, A., Dhaniyala, S., Korolev, A.; Eds. Wendisch, M., and Brenguier, J.-L.: Aerosol and Cloud Particle Sampling, In: Airborne Measurements for Environmental Research: Methods and Instruments, Ed. Wendisch, M. and Brenguier, J.-L., Wiley-VCH Verlag GmbH & Co. KGaA, https://doi.org/10.1002/9783527653218.ch6, 2013.

Lawson, R., O'Connor, D., Zmarzly, P., Weaver, K., Baker, B., Mo, Q., and Jonsson, H.: The 2D – S (Stereo) probe: Design and preliminary tests of a new airborne, high – speed, high – resolution particle Imaging probe, J. Atmos. Ocean. Technol., 23, 1462 – 1477, 2006.

Luebke, A., Avallone, L., Schiller, C., Meyer, J., Rolf, C., and Krämer, M.: Ice water content of Arctic, midlatitude, and tropical cirrus – Part 2: Extension of the database and new statistical analysis, ACP, 13, 6447–6459, 2013.

Luebke, A. E., Afchine, A., Costa, A., Grooss, J.-U., Meyer, J., Rolf, C., Spelten, N., Avallone, L. M., Baumgardner, D., and Krämer, M.: The origin of midlatitude ice clouds and the resulting influence on their microphysical properties, Atmospheric Chemistry and Physics, 16, 5793–5809, https://doi.org/10.5194/acp-16-5793-2016, 2016.

Mertes, S., Verheggen, B., Walter, S., Connolly, P., Ebert, M., Schneider, J., Bower, K. N., Cozic, J., Weinbruch, S., Baltensperger, U., and Weingartner, E.: Counterflow virtual impact or based collection of small ice particles in mixed-phase clouds for the physico-chemical characterization of tropospheric ice nuclei : Sampler description and first case study, AEROSOL SCIENCE AND TECHNOLOGY, 41, 848–864, https://doi.org/10.1080/02786820701501881, 2007.

Meyer, J.: Ice Crystal Measurements with the New Particle Spectrometer NIXE-CAPS, Schriften des Forschungszentrums Jülich. Reihe Energie und Umwelt / Energy and Environment; 160; ISBN:9783893368402, 2012.

Meyer, J., Rolf, C., Schiller, C., Rohs, S., Spelten, N., Afchine, A., Zöger, M., Sitnikov, N., Thornberry, T., Rollins, A., Gao, R., Bozoki, Z., Tatrai, D., Buchholz, B., Ebert, V., Mackrodt, P., Möhler, O., Saathoff, H., Rosenlof, K., and Krämer, M.: Two decades of water vapor measurements with the FISH fluorescence hygrometer: A review., ACP, 15, 8521–8538, https://doi.org/10.5194/acp-15-8521-2015, 2015, 2015.

Mitchell, D. L., D'Entremont, R. P., and Lawson, R. P.: Inferring Cirrus Size Distributions through Satellite Remote Sensing and Microphysical Databases, Journal of the Atmospheric Sciences, 67, 1106–1125, https://doi.org/10.1175/2009JAS3150.1, 2010.

Rollins, A. W., Thornberry, T. D., Gao, R. S., Smith, J. B., Sayres, D. S., Sargent, M. R., Schiller, C., Krämer, M., Spelten, N., Hurst, D. F., Jordan, A. F., Hall, E. G., Vömel, H., Diskin, G. S., Podolske, J. R., Christensen, L. E., Rosenlof, K. H., Jensen, E. J., and Fahey, D. W.: Evaluation of UT/LS hygrometer accuracy by intercomparison during the NASA MACPEX mission, JGR, 119, 1915–1935, https://doi.org/doi:10.1002/2013JD020817, 2014.

Schiller, C., Krämer, M., Afchine, A., Spelten, N., and Sitnikov, N.: Ice water content in Arctic, midlatitude and tropical cirrus, J. Geophys. Res., 113, D24208, https://doi.org/doi:10.1029/2008JD010342., 2008.

Smit, H., Krämer, M., Petzold, A., Rolf, C., Spelten, N., Rohs, S., Neis, P., Ebert, V., Buchholz, B., Bozoki, Z., Tatrai, D., Jones, R., Mead, M., and Malinowski, S.: Development and evaluation of novel compact hygrometers for airborne research (DENCHAR): Assessment report on the performance of the suite of hygrometers and recommendations, Eufar research report, Forschungszentrum Jülich, Jülich, Germany, 2013.

Thornberry, T., Rollins, A., Avery, M., Woods, S., Lawson, R., Bui, T., and Gao, R.-S.: Ice water content-extinction relationships and effective diameter for TTL cirrus derived from in situ measurements during ATTREX 2014, J. Geophys. Res., 122, 4494–4507, https://doi.org/10.1002/2016JD025948, 2017.

Vance, A. K., Abel, S. J., Cotton, R. J., and Woolley, A. M.: Performance of WVSS-II hygrometers on the FAAM research aircraft, Atmospheric Measurement Techniques, 8, 1617–1625, https://doi.org/10.5194/amt-8-1617-2015, https://www.atmos-meas-tech.net/8/1617/2015/, 2015.

Voigt, C., Schumann, U., Minikin, A., Abdelmonem, A., Afchine, A., Borrmann, S., Boettcher, M., Bucuchholz, B., Bugliaro, L., Costa, A., Curtius, J., Dollner, M., Doernbrack, A., Dreiling, V., Ebert, V., Ehrlich, A., Fix, A., Forster, L., Frank, F., Fuetterer, D., Giez, A., Graf, K., Grooss, J.-U., Gross, S., Heimerl, K., Heinold, B., Hueneke, T., Jaervinen, E., Jurkat, T., Kaufmann, S., Kenntner, M., Klingebiel, M., Klimach, T., Kohl, R., Krämer, M., Krisna, T. C., Luebke, A., Mayer, B., Mertes, S., Molleker, S., Petzold, A., Pfeilsticker, K., Port, M., Rapp, M., Reutter, P., Rolf, C., Rose, D., Sauer, D., Schaefer, A., Schlage, R., Schnaiter, M., Schneider, J., Spelten, N., Spichtinger, P., Stock, P., Walser, A., Weigel, R., Weinzierl, B., Wendisch, M., Werner, F., Wernli, H., Wirth, M., Zahn, A., Ziereis, H., and Zoger, M.: ML-Cirrus the airborne experiment on natural cirrus and contrail cirrus with the high-altitude long-range research aircraft HALO, Bulletin of the American Meteorological Society, 98, 271–288, https://doi.org/10.1175/BAMS-D-15-00213.1, 2017.

Wendisch, M. and Brenguier, J.-L. E.: Airborne Measurements for Environmental Research: Methods and Instruments, Wiley-VCH Verlag GmbH & Co. KGaA, ISBN:13:978-352740996, 2013.

Zöger, M., Afchine, A., Eicke, N., Gerhards, M.-T., Klein, E., McKenna, D., Mörschel, U., Schmidt, U., Tan, V., Tuitjer, F., Woyke, T., and Schiller, C.: Fast in situ stratospheric hygrometers: A new family of balloon-borne and airborne Lyman- photofragment fluorescence hygrometers., J. Geophys. Res., 104, 1807–1816, 1999.

Atmos. Meas. Tech. Discuss., https://doi.org/10.5194/amt-2017-373
Manuscript under review for journal Atmos. Meas. Tech.
Discussion started: 17 October 2017

Atmospheric Measurement Techniques Discussions

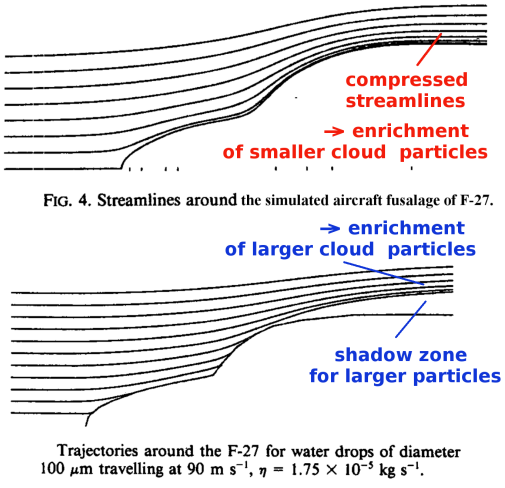

FIG. 4. Streamlines around the simulated aircraft fusalage of F-27.

Trajectories around the F-27 for water drops of diameter 100 μm travelling at 90 m s^{-1}, $\eta = 1.75 \times 10^{-5}$ kg s^{-1}.

Figure 1. Two-dimensional potential flow simulations of gas streamlines and particle trajectories around an aircraft shaped body, adapted from King (1984) (with annotations).

Atmos. Meas. Tech. Discuss., https://doi.org/10.5194/amt-2017-373
Manuscript under review for journal Atmos. Meas. Tech.
Discussion started: 17 October 2017

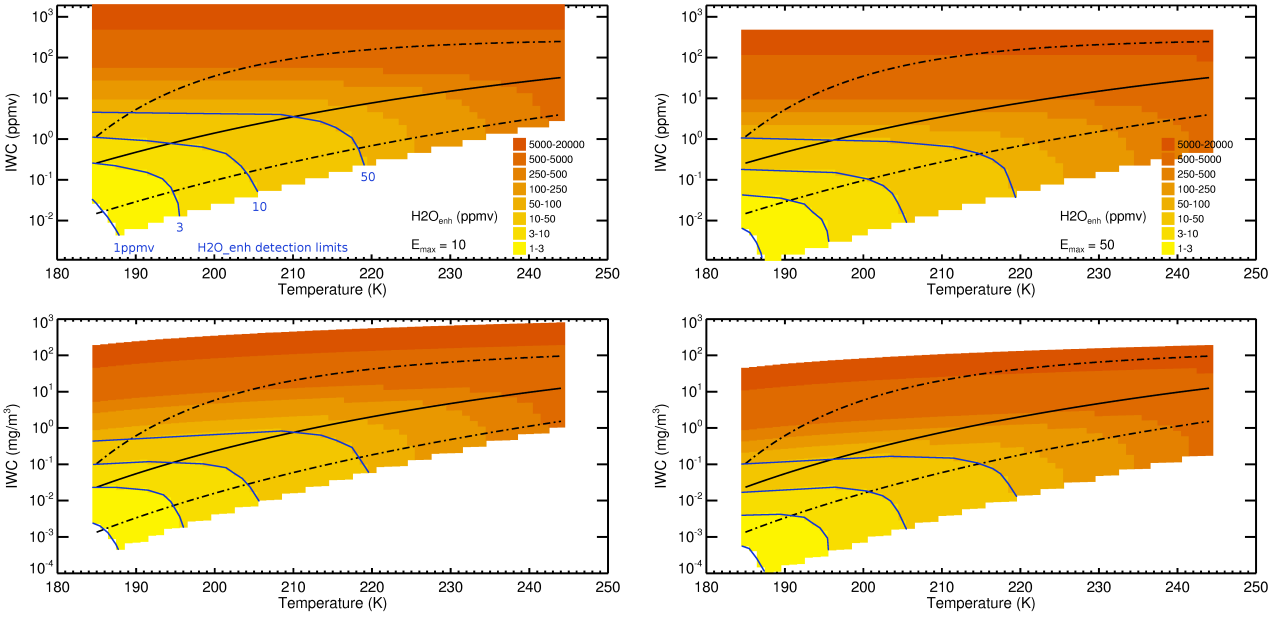

Figure 2. Relation between H_2O_{enh} and IWC in dependence of temperature for given H_2O_{gas} (assumed as water vapor saturation value), calculated from Eq. 1 ($IWC = \frac{H_2O_{enh} - H_2O_{gas}}{E_{max}}$) for two different E_{max} (left: 10, right: 50); top: volume mixing ratio, bottom: concentration). The minimum difference between H_2O_{enh} and H_2O_{gas} to detect IWC is 5% to account for measurement uncertainties, i.e. in the white region below the calculated IWCs, $H_2O_{enh}/H_2O_{gas} < 1.05$. Blue lines: H_2O_{enh} isolines corresponding to the detection limit of an instrument, e.g. the '1ppmv' and '3ppmv' H_2O_{enh} isolines represent the IWC detection limit of the FISH and HAI instruments described in Section 3.1.2. Black solid and dashed lines: medium, core max and min IWCs after Schiller et al. (2008).

Atmos. Meas. Tech. Discuss., https://doi.org/10.5194/amt-2017-373
Manuscript under review for journal Atmos. Meas. Tech.
Discussion started: 17 October 2017

Figure 3. Roof mounted FISH, HAI, Waran inlet at HALO (photos: top A. Fix, bottom A. Afchine).

Figure 4. Side mounted FISH-inlet at Geophysica (photo: A. Afchine).

Figure 5. Bottom mounted FISH-inlet at WB-57 (photo: A. Afchine).

Atmos. Meas. Tech. Discuss., https://doi.org/10.5194/amt-2017-373
Manuscript under review for journal Atmos. Meas. Tech.
Discussion started: 17 October 2017

Atmospheric Measurement Techniques Discussions

Figure 6. NIXE underwing mounting at HALO (photo: A. Afchine).

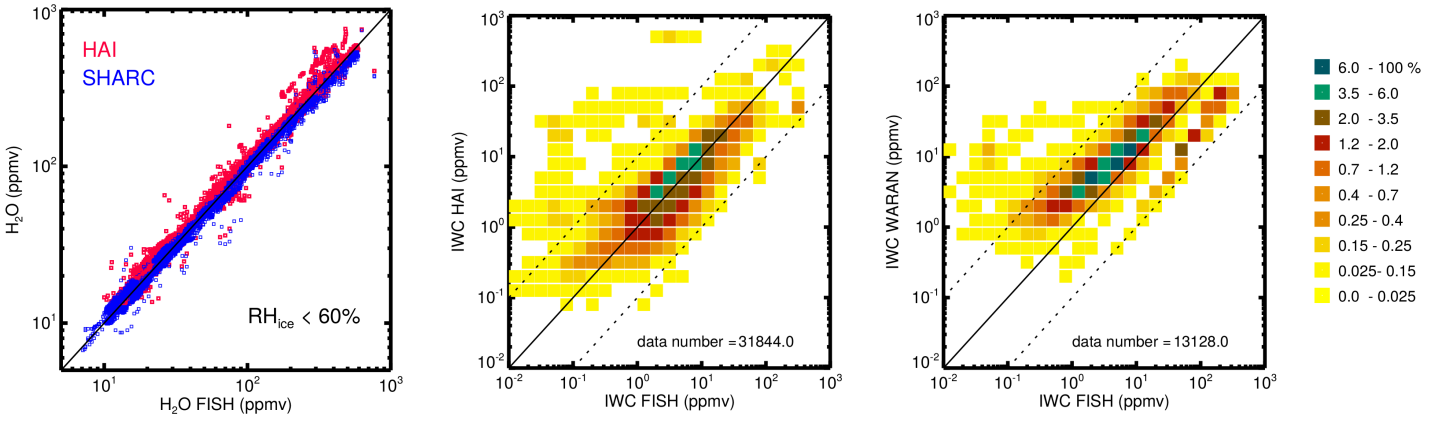

Figure 7. Comparison of H_2O and IWCs from roof-mounted closed-path hygrometers FISH and HAI (H_2O_{tot}) and SHARC (H_2O_{gas}) @HALO during ML-CIRRUS 2014 (color code: frequencies; solid black: 1:1 line; dashed: $\pm$ factor 10 to 1:1 line).

Atmos. Meas. Tech. Discuss., https://doi.org/10.5194/amt-2017-373
Manuscript under review for journal Atmos. Meas. Tech.
Discussion started: 17 October 2017

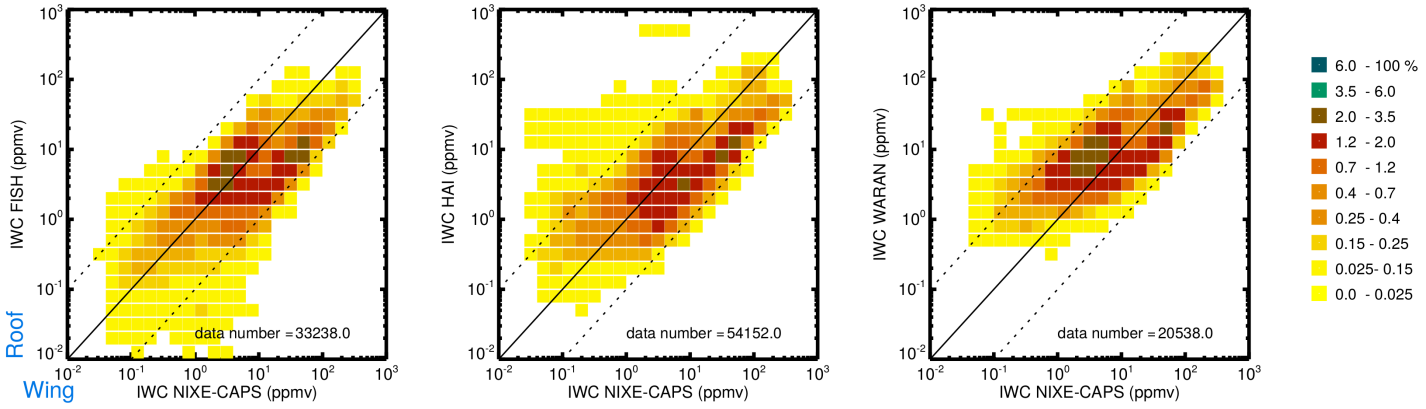

Figure 8. Comparison of IWCs from roof-mounted closed-path hygrometers FISH, HAI and Waran (see Equation 1, H_2O_{gas} from SHARC) and wing-mounted cloud spectrometer NIXE @HALO during ML-CIRRUS 2014 (color code: frequencies; solid black: 1:1 line; dashed: $\pm$ factor 10 to 1:1 line).

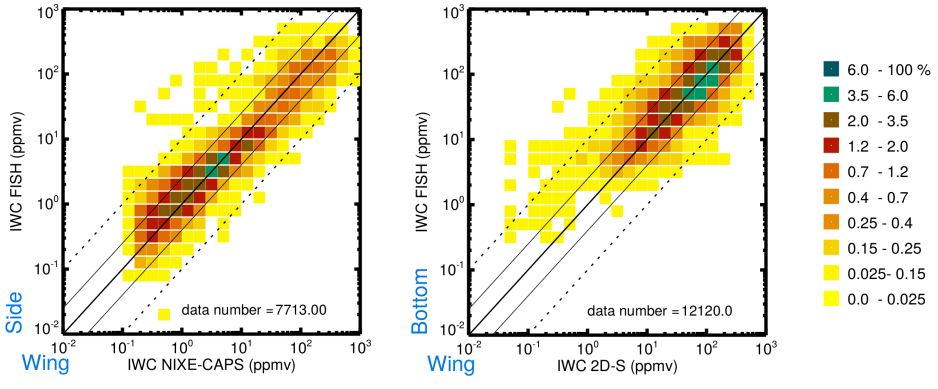

Figure 9. Comparison of IWCs from left: side mounted closed-path FISH (see Equation 1, H_2O_{gas} from FLASH) and wing-mounted cloud spectrometer NIXE @Geophysica during StratoClim 2017; right: bottom-mounted closed-path FISH (see Equation 1, H_2O_{gas} from HWV) and wing-mounted cloud spectrometer 2D-S @WB-57 during MacPex 2011 (color code: frequencies; solid black: 1:1 line; dashed/thin: $\pm$ factor 10/2.5 to 1:1 line).

Atmos. Meas. Tech. Discuss., https://doi.org/10.5194/amt-2017-373
Manuscript under review for journal Atmos. Meas. Tech.
Discussion started: 17 October 2017

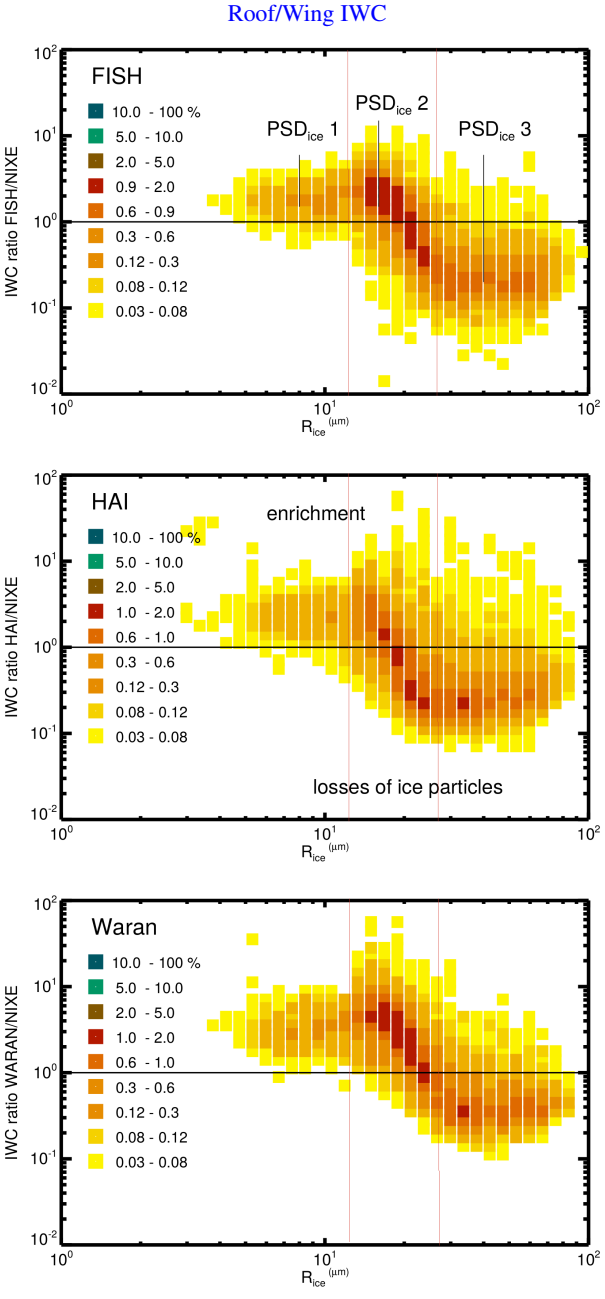

Figure 10. Ratios of Roof/Wing IWC (Roof IWC from FISH, HAI, Waran; Wing IWC from NIXE) vs. mean mass R_{ice}.

Atmos. Meas. Tech. Discuss., https://doi.org/10.5194/amt-2017-373
Manuscript under review for journal Atmos. Meas. Tech.
Discussion started: 17 October 2017

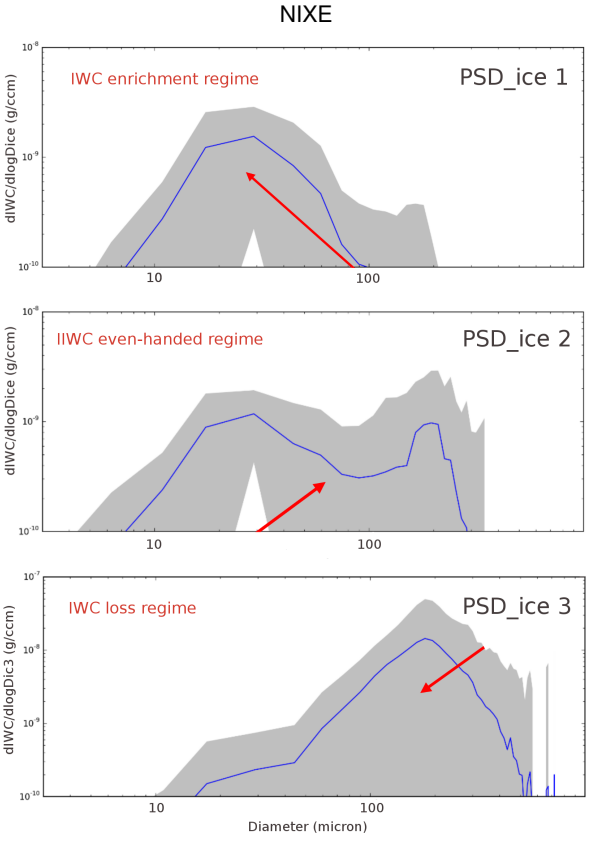

Figure 11. Three types of cirrus mass size distributions dIWC/dlogD_{ice}, exemplarily for the flight on 4. April 2014. Blue lines represent the mean PSDs, the grey area the standard deviation; note that for the portrayal of the PSD we use the ice particle diameter and not radius to clearly distinguish from the mean mass radius R_{ice} of the ice particle population used in Figures 10.

Atmos. Meas. Tech. Discuss., https://doi.org/10.5194/amt-2017-373
Manuscript under review for journal Atmos. Meas. Tech.
Discussion started: 17 October 2017

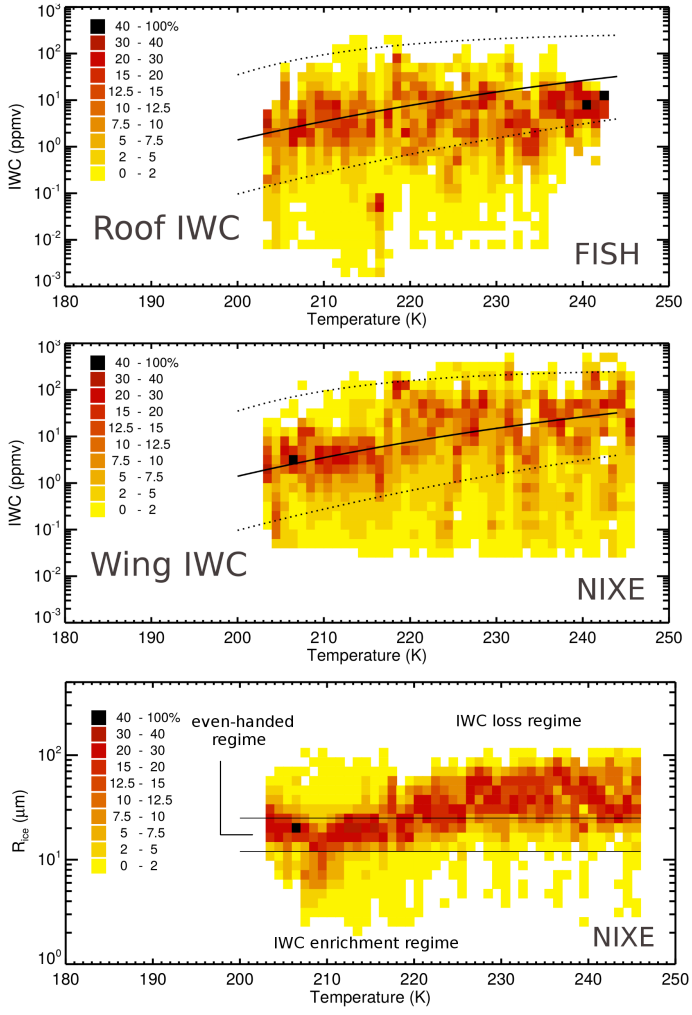

Figure 12. Top and middle panel: IWC and in dependence o temperature during ML-CIRRUS 2014, from roof-mounted FISH and wing-mounted NIXE (color code: frequencies of occurrence, black solid and dashed lines: median, core min. and max. IWCs after Schiller et al., 2008). Bottom panel: R_{ice} in dependence of temperature during ML-CIRRUS 2014, from wing-mounted NIXE (the black lines denote the size regimes where ice particles are lost, enriched or both, for detail see Section 4.2).